FAILURE OF FIBER-REINFORCED GRANULAR SOILS

By Radoslaw L. Michalowski,[1] Member, ASCE, and Aigen Zhao,[2] Associate Member, ASCE

ABSTRACT: Short fibers have been tried in the past few years as a soil-improvement admixture (reinforcement), yet no failure criteria for fiber-reinforced soils, consistent with numerical methods for solving boundary-value problems, are available. An attempt at deriving the limit condition for a fiber-reinforced granular soil is presented. An energy-based homogenization scheme is used to arrive at the macroscopic failure stress of the fibrous granular composite. A piecewise closed-form failure criterion is derived. The internal friction angle is used to quantify the strength of the granular matrix, and the fibers are characterized by volumetric concentration, aspect ratio, yield point, and the fiber-soil interface friction angle. Laboratory tests on specimens with low fiber content indicate a good agreement of the model predictions with the actual test results.

INTRODUCTION

The concept of reinforcing soils with tension-resisting elements has been widely accepted in engineering practice. Reinforcement elements in the form of long metal strips or sheets of geosynthetic fabric (or geogrid) are typical of traditional soil-improvement techniques. Less attention has been paid to nontraditional reinforcement, such as continuous filament or short fibers. Approximate methods for the design of structures with traditionally reinforced soil exist, whereas no techniques are available for design with fiber-reinforced soils. This is mainly due to a poor understanding of the fiber-matrix (filament-matrix) interaction and, consequently, a lack of appropriate models capable of describing the stress-strain behavior and failure of such composites.

This paper presents an attempt at describing the failure of fiber-reinforced granular soil. In particular, a mathematical description of a failure criterion for fiber-reinforced soil in a macroscopic stress space is presented. Experimental results are shown to demonstrate the adequacy of the theoretical description proposed, and to indicate the imminent direction in further development of the model.

The earlier work in the area of fiber-reinforced soils is briefly mentioned in the next section, followed by a brief description of the homogenization technique used here, and the derivation of the macroscopic stress state associated with the composite (fiber-reinforced soil) failure. Results from triaxial drained tests on specimens of fiber-reinforced soil are also presented, and the paper ends with concluding remarks.

PREVIOUS WORK

A rational approach to the description of the behavior of composite materials is based on introducing macroscopic properties. The term "macroscopic" pertains here to global (or average) properties of the mixture, and is not an indication of size. Mechanical properties of composite materials are then described using various methods of homogenization (averaging). These include self-consistent schemes [see, for instance, Hill (1965), Budiansky (1965), Mori and Tanaka (1973)] or numerical procedures, such as the finite-element method (FEM) [for instance, Dvorak et al. (1974)]. An excellent survey of techniques used for the analysis of composite materials was presented by Hashin (1983).

Although a significant interest in fiber composites has been maintained in the last few decades, little attention has been paid to composites with granular or low-cementitious matrices. There is a handful of papers with results of tests on specimens of fiber-reinforced soils (Andersland and Khattak 1979; Hoare 1979; Arenicz and Chowdhury 1988; Gray and Ohashi 1983; Maher and Gray 1990). An attempt at describing the strength was made by Gray and Ohashi (1983) and Maher and Gray (1990) through considerations of soil-fiber interaction in a localized shear band. These attempts follow earlier efforts by Waldron (1977) and Wu et al. (1979), where the influence of tree roots intersecting failure surfaces of slopes was considered. Such an approach, while appropriate for estimating the safety of slopes, may not be very suitable for evaluating the soil strength increase due to fibers. The former is a boundary-value problem in which the roots are considered as an additional structural component, while the latter is a constitutive modeling concern. Strain localization is a bifurcation phenomenon where the response of the specimen is no longer representative of unique material properties, because the deformation mode (and the evolution of properties) is no longer uniform.

There is no analytical description of the macroscopic stress state at failure, which is consistent with the principles of constitutive modeling and is applicable in numerical methods for solving boundary-value problems with fiber-reinforced soils. There are attempts at the description of the uniaxially reinforced soil (Sawicki 1983; de Buhan et al. 1989; Michalowski and Zhao 1993), but analytical data on the failure criteria of continuous filament or fiber-reinforced soil is rather scarce (di Prisco and Nova 1993; Michalowski and Zhao 1994). This paper is a continuation of efforts toward constructing a consistent model to predict the failure of fiber-reinforced soils.

HOMOGENIZATION PROCEDURE

An energy-based homogenization technique is used here to calculate the macroscopic stress state of fiber-reinforced sand at failure. In this approach to homogenization, an incipient deformation for a representative element, such as the one in Fig. 1(a), is assumed first. Next, the energy dissipation rate, $D(\dot{\varepsilon}_{ij})$, in the soil and fibers is calculated during the incipient deformation process, and it is equated to the work rate of the macroscopic stress $\bar{\sigma}_{ij}$

$$\bar{\sigma}_{ij}\bar{\dot{\varepsilon}}_{ij} = \frac{1}{V}\int_v D(\dot{\varepsilon}_{ij})\, dV \tag{1}$$

where V = volume of a representative element of the composite; and $\bar{\dot{\varepsilon}}$ = macroscopic (average) strain rate. A similar averaging technique was investigated earlier in the context of cementitious composites by Hashin (1964) and Shu and Rosen (1967), and, for two-dimensional membranes, by McLaughlin and Batterman

[1]Assoc. Prof., Dept. of Civ. Engrg., The Johns Hopkins Univ., Baltimore, MD 21218.

[2]Des. Engr., Tenax Corp., 4800 East Monument St., Baltimore, MD 21205.

Note. Discussion open until August 1, 1996. To extend the closing date one month, a written request must be filed with the ASCE Manager of Journals. The manuscript for this paper was submitted for review and possible publication on December 27, 1994. This paper is part of the ***Journal of Geotechnical Engineering***, Vol. 122, No. 3, March, 1996. ISSN 0733-9410/96/0003-0226–0234/$4.00 + $.50 per page. Paper No. 9842.

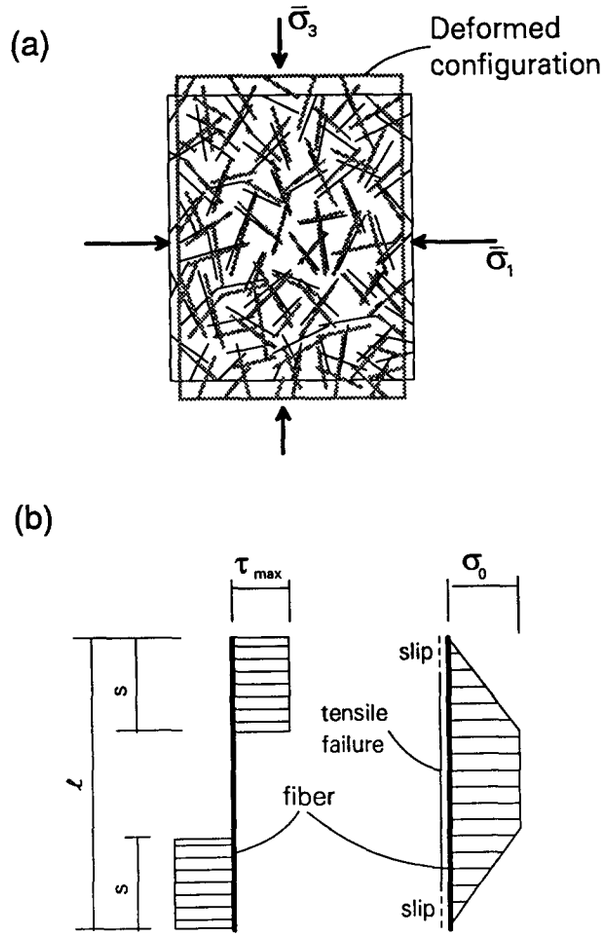

FIG. 1. Fiber-reinforced Composite: (a) Plane-Strain Deformation of 3D Specimen; (b) Fiber-Matrix Shear Stress and Axial Stress in Rigid–Perfectly Plastic Fiber

(1970). It was also used to homogenize a unidirectionally reinforced sand (Michalowski and Zhao, 1995).

The specific deformation pattern assumed here in the homogenization process has a linear distribution of velocities, subject to constraints imposed by the dilatancy of the base (matrix) material (such as in Michalowski and Zhao, 1995). It is further assumed that the deformation rate of the granular matrix is identical to the macroscopic deformation ($\dot{\varepsilon}_{ij} = \dot{E}_{ij}$). The fibers are considered one-dimensional elements, and they can deform at the same rate (on reaching yield stress), or, they can slip in the matrix.

FAILURE CRITERION FOR FIBER-REINFORCED SOIL

Definitions and Assumptions

We assume here that the fibers are distributed uniformly in the space with a random distribution of orientation. Hence, a representative specimen must exist in which the fiber concentration ρ and the distribution of orientation can be considered uniform. Fiber concentration characterizes the amount of reinforcement and is defined here as follows:

$$\rho = \frac{V_r}{V} \tag{2}$$

where V_r = volume of the fibers; and V = volume of the entire representative composite element. For practical purposes, such as preparing specimens of fiber-reinforced soil, the weight content may be a more convenient parameter. However, as the mechanical properties of the composite constituents are not necessarily related to their mass densities (and, therefore, to the unit weights), the volumetric content of the fibers is the appropriate parameter to represent the fiber content. It is the volumetric content of the constituents that governs the averaging schemes in the theory of mixtures.

The fibers are considered to be cylindrical in shape, and their slenderness is described here by the aspect ratio

$$\eta = \frac{l}{2r} \tag{3}$$

where l = length of the fiber; and r = its radius. It is further understood that the length of the fibers is at least one order of magnitude larger than the diameter (say d_{50}) of the sand grains, and the diameter of fibers is at least of the same order as the grains.

Both the fibers and matrix (granular fill) are considered perfectly plastic, described by the Tresca and the Mohr-Coulomb failure criteria, respectively. The influence of the confining stress on the fiber tensile strength is ignored. The kinematics of the granular fill is governed by the normality rule.

Contribution of Fibers to Strength of Composite

Failure of a single fiber in a deforming composite can occur due to fiber slip or tensile rupture. Tensile rupture will be modeled here as the incipient plastic flow of fibers. However, even if a tensile rupture occurs, the ends of the fiber will slip as the tensile strength of the fiber material cannot be mobilized throughout the entire fiber length. For a rigid–perfectly plastic behavior of the granular soil, fibers, and interface, the expected distribution of the shear stress on the fiber surface and the axial stress in the fiber must conform to that shown in Fig. 1(b).

When a fiber fails in the tensile rupture mode, the slip occurs at both fiber ends up to the distance s, as follows:

$$s = \frac{r}{2} \frac{\sigma_0}{\sigma_n \tan \varphi_w} \tag{4}$$

where σ_0 = yield stress of the fiber material; σ_n = stress normal to the fiber surface; and φ_w = friction angle of the matrix-fiber interface. A pure slip failure mode will occur if the length of fibers l becomes less than $2s$, or when the aspect ratio is

$$\eta < \frac{1}{2} \frac{\sigma_0}{\sigma_n \tan \varphi_w} \tag{5}$$

We further assume that the fibers contribute to the strength of the composite only if they are subjected to tension, whereas their influence in the compressive regime is neglected due to possible buckling and kinking.

Deformation of an Idealized Specimen and Integration Space with "Ordered" Fibers

A plane-strain deformation is considered here for the specimen depicted in Fig. 1(a), with a linear velocity distribution. The volume of the specimen is large enough so that its increase does not produce any change in the average properties of the specimen (representative volume).

The consequence of the linear velocity field is a uniform strain rate throughout the specimen. The deformation process assumed is irreversible (plastic flow) and is interpreted here as a composite failure. The average stress (macroscopic stress state) at failure is obtained from (1). The kinematics of the granular fill is governed by the flow rule associated with the Mohr-Coulomb yield condition, which leads to the following constraint on dilatancy (plane strain):

$$\frac{\dot{\varepsilon}_1 + \dot{\varepsilon}_3}{\dot{\varepsilon}_1 - \dot{\varepsilon}_3} = -\sin \varphi \quad \text{or} \quad \frac{\dot{\varepsilon}_1}{\dot{\varepsilon}_3} = -\tan^2\left(\frac{\pi}{4} - \frac{\varphi}{2}\right) \tag{6a,b}$$

where $\dot{\varepsilon}_1$ and $\dot{\varepsilon}_3$ = maximum and minimum principal strain rates, respectively; and φ = internal friction angle of the matrix (for the associative flow rule, φ also indicates the rate of dilation).

To make integration on the right-hand side of (1) tractable, we introduce a space with "ordered" fibers (Fig. 2) where all fibers are moved (in a parallel manner) to the origin of that space. Such transformation is admissible since the energy dissipation rate in fibers is dependent only on their orientation, and is independent of their location in the sample. The sample from Fig. 1(a) (which is three-dimensional, with fibers oriented in three-dimensional space) is now represented by a sphere with radius R_0 (fibers are not shown in Fig. 2). Due to macroscopic isotropy of the composite and symmetry of the deformation pattern, it is sufficient to consider one-eighth of the sphere.

Energy Dissipation Rate in an Idealized Specimen

The energy dissipation rate during plastic deformation of soil conforming to the Mohr-Coulomb failure condition and associative flow rule is zero; therefore, only the fibers will contribute to the dissipation in the composite specimen.

First, the region of fibers under compression in space in Fig. 2 needs to be found. A uniform plane deformation is considered, with the x- and y-axes (Fig. 2) coinciding with directions 1 and 3 [Fig. 1(a)], respectively. The regions with fibers in tension and compression are separated by a plane of inclination θ_0 (plane OBC in Fig. 2). All fibers in plane OBC undergo no deformation

$$\dot{\varepsilon}_{\theta_0} = \dot{\varepsilon}_1 \cos^2\theta_0 + \dot{\varepsilon}_3 \sin^2\theta_0 = 0 \tag{7}$$

which leads to

$$\frac{\dot{\varepsilon}_1}{\dot{\varepsilon}_3} = -\tan^2\theta_0 \tag{8}$$

and, considering (6), angle θ_0 can be determined as

$$\theta_0 = \frac{\pi}{4} - \frac{\varphi}{2} \tag{9}$$

The energy dissipation rate in a single fiber oriented in direction θ, due to slip along end sections s and plastic extension in the middle section of length $l - 2s$, is

$$d = 2\pi r s^2 \sigma_n \tan\varphi_w \langle\dot{\varepsilon}_\theta\rangle + \pi r^2 (l - 2s)\sigma_0 \langle\dot{\varepsilon}_\theta\rangle$$

$$= \pi r^2 \sigma_0 \left(l - \frac{r\sigma_0}{2\sigma_n \tan\varphi_w}\right) \langle\dot{\varepsilon}_\theta\rangle \tag{10}$$

Since the number of fibers per unit volume of the composite is $\rho/\pi r^2 l$, the energy dissipation rate in fibers per unit volume of the composite is

$$D_r = \frac{1}{V}\int_v \pi r^2 \sigma_0 \left(l - \frac{r\sigma_0}{2\bar{\sigma}_n \tan\varphi_w}\right) \frac{\rho}{\pi r^2 l} \langle\dot{\varepsilon}_\theta\rangle \, dV \tag{11}$$

where $\bar{\sigma}_n$ = average normal stress to the fibers in volume V; and $\langle\dot{\varepsilon}_\theta\rangle$ = strain rate in the direction of the fiber (tension is taken here as negative)

$$\langle\dot{\varepsilon}_\theta\rangle = \begin{cases} |\dot{\varepsilon}_\theta| & \text{if } \dot{\varepsilon}_\theta < 0 \\ 0 & \text{otherwise} \end{cases} \tag{12}$$

The energy dissipation rate per unit volume of the composite from (11) can be written as

$$D_r = \frac{1}{\frac{1}{6}\pi R_0^3} \int_v \left(1 - \frac{1}{4\eta} \frac{\sigma_0}{\bar{\sigma}_n \tan\varphi_w}\right) \rho\sigma_0 \langle\dot{\varepsilon}_\theta\rangle \, dV \tag{13}$$

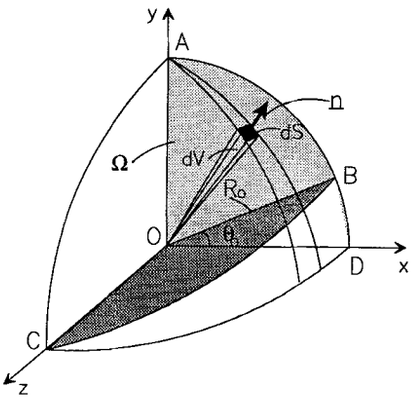

FIG. 2. Integration Space with "Ordered" Fibers (Fibers not Shown)

where dV = an infinitesimal volume shown in Fig. 2. The exact magnitude of the average stress normal to the soil/fiber interface cannot be found since the distribution of the microstress is not considered here. An approximation is made where $\bar{\sigma}_n$ is assumed constant for all fibers, and equal to the mean of the maximum and minimum principal stress in the composite [$p = (\bar{\sigma}_1 + \bar{\sigma}_3)/2$]. Such an assumption is a realistic estimate of $\bar{\sigma}_n$ for randomly distributed fibers.

The integration of (13) is shown in Appendix I, and the result can be presented in the following form:

$$D_r = \frac{\rho\sigma_0}{3} M \left(1 - \frac{1}{4\eta} \frac{\sigma_0}{p \tan\varphi_w}\right) \dot{\varepsilon}_1 \tag{14}$$

where

$$M = \left(\frac{1}{2} + \frac{\varphi}{\pi} + \frac{1}{\pi}\cos\varphi\right) \tan^2\left(\frac{\pi}{4} + \frac{\varphi}{2}\right) - \frac{1}{2} - \frac{\varphi}{\pi} + \frac{1}{\pi}\cos\varphi \tag{15}$$

If the condition in (5) is satisfied, then pure slip occurs, and the foregoing procedure leads to an expression for the energy dissipation rate per unit volume independent of the fiber yield stress σ_0

$$D_r = \frac{1}{3}\rho\eta M p \tan\varphi_w \dot{\varepsilon}_1 \tag{16}$$

Failure Criterion for Fiber-Reinforced Soil

The energy balance (1) for isotropic material under plane-strain conditions is

$$\dot{\varepsilon}_1\bar{\sigma}_1 + \dot{\varepsilon}_3\bar{\sigma}_3 = D_r = \frac{\rho\sigma_0}{3} M \left(1 - \frac{1}{4\eta} \frac{\sigma_0}{p \tan\varphi_w}\right) \dot{\varepsilon}_1 \tag{17}$$

Utilizing (6), one obtains

$$\bar{\sigma}_1 - \tan^2\left(\frac{\pi}{4} + \frac{\varphi}{2}\right) \bar{\sigma}_3 = \frac{\rho\sigma_0}{3} M \left(1 - \frac{1}{4\eta} \frac{\sigma_0}{p \tan\varphi_w}\right) \tag{18}$$

Introducing stress invariant R, convenient for plane-strain conditions (radius of the Mohr circle)

$$R = \sqrt{\frac{(\bar{\sigma}_x - \bar{\sigma}_y)^2}{4} + \bar{\tau}_{xy}^2} \tag{19}$$

and noting that $2p = \bar{\sigma}_1 + \bar{\sigma}_3$, (18) can be transformed to represent the failure criterion of the fiber-reinforced soil in terms of in-plane invariants R and p

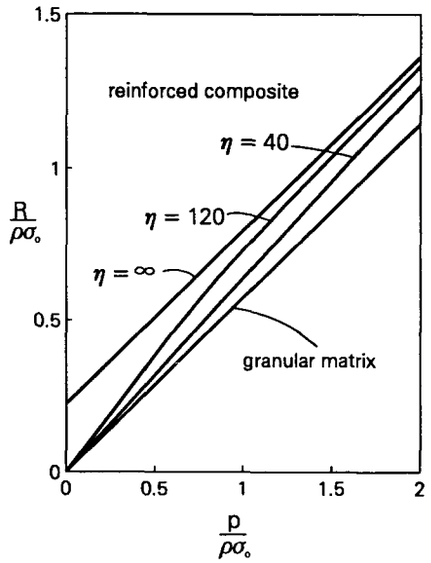

FIG. 3. Theoretical Failure Criterion for Granular Composite ($\rho = 0.02$, $\varphi = 35°$, $\varphi = 20°$)

$$\frac{R}{\rho\sigma_0} = \frac{p}{\rho\sigma_0}\sin\varphi + \frac{1}{3}N\left(1 - \frac{1}{4\eta\rho}\frac{\cot\varphi_w}{\frac{p}{\rho\sigma_0}}\right) \tag{20}$$

where

$$N = \frac{1}{\pi}\cos\varphi + \left(\frac{1}{2} + \frac{\varphi}{\pi}\right)\sin\varphi \tag{21}$$

When pure slip occurs [(5)] the failure criterion takes the form

$$\frac{R}{\rho\sigma_0} = \frac{p}{\rho\sigma_0}\left(\sin\varphi + \frac{1}{3}N\rho\eta\tan\varphi_w\right) \tag{22}$$

When no fibers are present both (20) and (22) reduce to the standard Mohr-Coulomb failure criterion for granular material

$$R = p\sin\varphi \tag{23}$$

Fig. 3 presents results from (20) and (22) in the R-p plane. Different curves present the failure criteria for fiber-reinforced soil with fibers of various aspect ratios. As indicated in (22), the slip mode is described by a linear function (when the internal friction angle of the soil fill is constant), whereas in the tensile rupture mode the shear strength is not proportional to the mean stress [(20)]. There is no discontinuity in the gradient at the transition point (smooth piecewise function). Stresses are normalized in Fig. 3 by parameter $\rho\sigma_0$ (fiber concentration $\times$ fiber yield point).

EXPERIMENTAL TESTS

An experimental investigation was carried out primarily to determine whether the approach selected for mathematical description of the failure criterion is reasonable, and, if so, to indicate where the refinement of the suggested failure condition should be pursued.

Material Used

A coarse, poorly graded sand with $d_{50} = 0.89$ mm and uniformity coefficient $C_u = 1.52$ was used in the experiments. The specific gravity of the sand was $G = 2.65$, and the minimum and maximum void ratios were 0.56 and 0.89, respectively. Two types of fibers were selected: galvanized or stainless steel ($G = 7.85$), and polyamide monofilament ($G = 1.28$). Polyamide is not a material likely to be used as a permanent soil reinforcement (because of its moisture sensitivity and aging/deterioration characteristics), but its availability in a variety of diameters and its mechanical behavior common to other synthetic materials makes it a convenient material to use in tests.

Compaction of the specimens was characterized by the void ratio. In all tests the initial void ratio of prepared specimens was $e = 0.66$, corresponding to a relative density of $I_d = 70\%$ for unreinforced sand. In the definition of the void ratio for reinforced specimens the volume of the fibers is considered part of the skeleton. Relative density is not an appropriate parameter for characterizing fiber-reinforced specimens, because the minimum and maximum void ratios of the composite are very much dependent on the fiber characteristics.

Specimen Preparation

The length of the fibers was approximately 25 mm in all tests, and the required aspect ratio was adjusted by selecting an appropriate fiber diameter. Both the height and diameter of the specimens was 96.5 mm. The following procedure of sample preparation was followed in order to achieve uniform distribution of fibers in space and isotropic distribution of fiber orientation in the specimens.

1. According to the required void ratio ($e = 0.66$) and fiber concentration by volume (ρ), the corresponding fiber concentration by weight (ρ_w) was calculated as

$$\rho_w = \frac{(1 + e)G_r\rho}{(1 + e)(G_r - G_s)\rho + G_s} \tag{24}$$

where G_s and G_r = specific gravity of the sand and fibers, respectively. The weight of the dry sand (W_s) and the fibers (W_r) was then calculated from

$$W_s = \frac{V}{1 + e}\frac{(1 - \rho_w)G_sG_r}{(1 - \rho_w)G_r + \rho_wG_s}\gamma_w \tag{25}$$

and

$$W_r = \frac{V}{1 + e}\frac{\rho_wG_sG_r}{(1 - \rho_w)G_r + \rho_wG_s}\gamma_w \tag{26}$$

where V = required volume of the mixture (volume of the specimen); and γ_w = specific weight of water.
2. The weight of the sand and fibers was divided into five equal portions used later to produce five layers of the specimen.
3. A 60 $\times$ 60 mm square grid of steel wires (with 30 mm spacing between the wires) was placed at the bottom of the mold.
4. A small amount of sand was dropped through a funnel into the mold to cover the grid evenly. Each of the five portions (second step in procedure) was divided into three parts. One-third of the fibers for the first layer was slowly dropped into the mold. Care was taken to produce an even distribution of the fibers on the sand surface. Then, one-third of the sand for that layer was dropped through a funnel with a low mass rate (fall-height = 0.4 m). Following the same procedure, the remaining two parts of the first layer of the specimen were produced.
5. The grid was slowly pulled (manually) through the first one-fifth portion of the specimen (first layer). The grid was left on the surface of that layer.
6. The distance from a reference point on the mold to the top of the layer was measured to ensure that the target void ratio was achieved. If the prepared mixture was too loose, the mixture was gently vibrated until the proper density was reached. If the mixture was significantly too

loose (or it was too dense), the entire specimen was recreated.

7. For the subsequent four layers of the specimen, steps 4–6 were repeated. The possible influence of vibration on the layers below, when preparing the subsequent layers, was ignored.

The same preparation procedure was followed for unreinforced specimens (except there were no fibers). The grid used in steps 3 and 5 was intended to create an isotropic distribution of fiber orientation. When placing the sand and fiber mixture directly into the mold, the fibers were assuming an anisotropic orientation with the horizontal being the preferred direction. Therefore, the sand and fiber mixture was placed over a grid of wires and the grid was pulled slowly through the mixture, altering the orientation of a portion of fibers. This technique was developed to assure an approximately uniform distribution of fiber orientation (macroscopically isotropic specimens). The distribution of fiber orientation was estimated to be isotropic by visual inspection, and the writers recognize the approximate quality of the conclusion.

Results

Series of triaxial tests were conducted. The fiber concentration, aspect ratio, diameter of fibers, and the range of confining pressure for these tests are given in Table 1. The typical confining pressures for one series were: 50, 100, 200, 300, 400, and 600 kN/m^2. The results of the tests are presented in Figs. 4–7.

The addition of steel fibers to sand led to an increase in the peak shear stress of about 20% (ρ = 1.25%, η = 40) for samples tested under a confining pressure of 100–600 kN/m^2 [Fig. 4(a)]; this relative increase was larger at a very low confining pressure (50 kN/m^2). The samples exhibited a typical compaction effect [Fig. 4(b), ε_v = volumetric strain] at small axial strains ε_1, and dilation at larger strains. The presence of fibers inhibited the dilation effect to a certain degree. The increase in the content of steel fibers (ρ) leads to a clear increase in the peak shear stress [Fig. 5(a)], and, also leads to an increase in the stiffness of the composite prior to reaching failure. An increase in the aspect ratio of the fibers contributes to a significant increase in the peak shear stress [Fig. 5(b)].

Polyamide fibers produced a significant increase in the peak shear stress [Fig. 6(a)] for large confining pressures, but the effect is associated with a considerable loss of stiffness prior to failure and a substantial increase of the strain to failure. At a confining pressure of 100 kN/m^2, however, no increase of the peak shear (with respect to the granular matrix alone) was recorded.

Addition of the polyamide fibers to the soil inhibits the dilatancy, and the effect is more pronounced for low confining pressures [Fig. 6(b)]. An increase in the fiber content, while the aspect ratio is kept constant, leads to a very significant increase in the peak shear stress, a noticeable decrease in stiffness, and an increase of the strain to failure [Fig. 7(a)]. An increase in the aspect ratio of polyamide fibers leads to similar effects [Fig. 7(b)].

ANALYSIS OF EXPERIMENTS AND THEORETICAL PREDICTIONS

A one-to-one height-to-diameter ratio of the specimens led to failure where no visible localization of strain was present. The extra care taken to minimize the effect of friction at the bases of specimens allows one to assert that the macroscopic stress in the composite specimens was close to uniform, and the measured deviatoric stress at failure can be identified with the failure stress of the composite material (macroscopic failure stress state). These stresses, therefore, can be compared directly to those predicted by the suggested theory.

TABLE 1. Specimens Tested

Fiber material (1)	Fiber concentration ρ (%) (2)	Aspect ratio η (3)	Fiber diameter $2r$ (mm) (4)	Range of confining pressure σ_3 (kN/m^2) (5)
No fibers	0	—	—	50–600
Steel	0.41	40	0.64	100–600
Steel	1.25	40	0.64	50–600
Steel	0.5	85	0.3	50–600
Polyamide	0.5	85	0.3	50–600
Polyamide	1.25	85	0.3	400
Polyamide	0.5	180	0.14	400

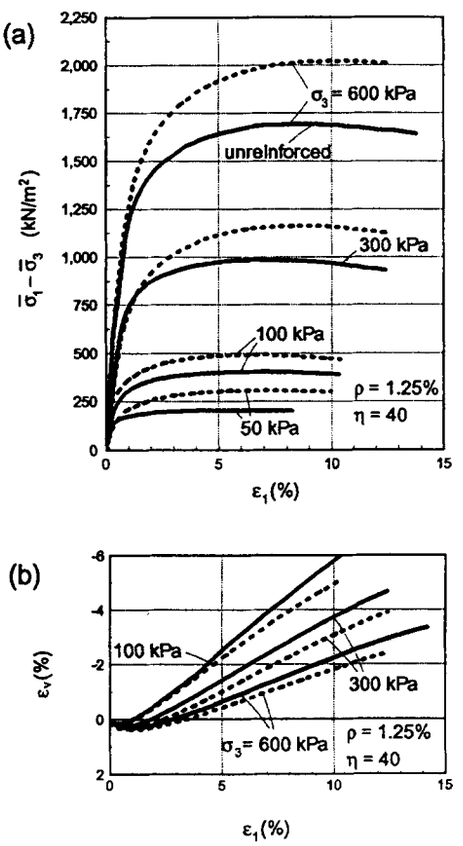

FIG. 4. Triaxial Compression Tests on Sand Reinforced with Steel Fibers: (a) Stress-Strain Relation for Different Confining Pressures; (b) Volumetric Strain

The use of different deformation modes in the theoretical derivation (plane strain) and in the experiments (axisymmetrical kinematics) may be disputed by some. The matrix failure criterion used (Mohr Coulomb) is independent of the intermediate principle stress, and the theoretical result is not affected by whether the matrix deformation is plain or axisymmetrical. However, the particular deformation mode used in the homogenization process does affect the theoretical result through the fiber component, when only fibers in the tensile regime are considered to contribute to the composite strength. This is because the volumetric strain rate associated with fibers in tension is not invariant, only the total volumetric strain rate is. As a result of further theoretical considerations, this effect appeared to be small (negligible).

Although the influence of the mean principal stress on the granular matrix strength is not contested [see, for instance, Lade (1977)], the model presented is a reasonable approxi-

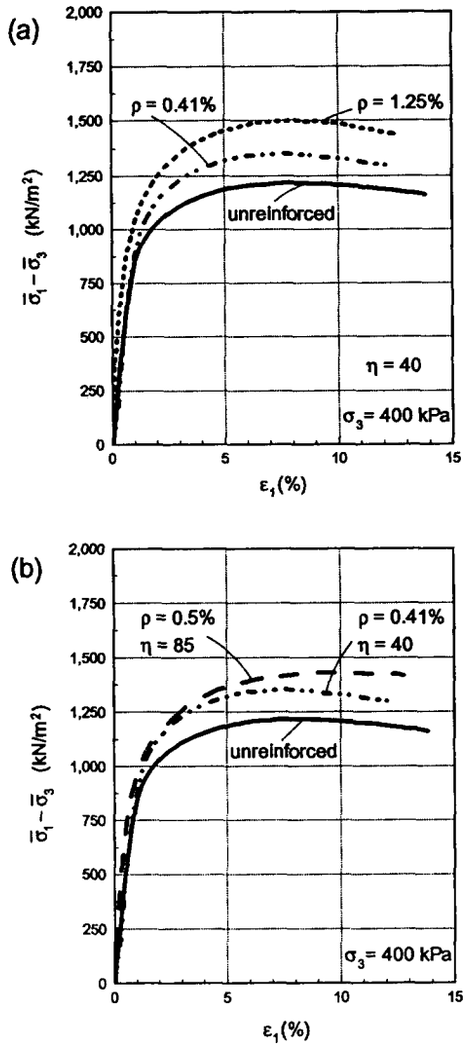

FIG. 5. Stress-Strain Behavior of Steel Fiber-Reinforced Sand: (a) Influence of Fiber Content; (b) Effect of Fiber Aspect Ratio

mation of the true composite behavior. To reduce the influence of the granular matrix approximation (Mohr-Coulomb criterion) in the theory-experiment comparison, the internal friction angle of the matrix used for theoretical prediction was determined from the axisymmetrical (triaxial compression) tests, and the composite specimens were also tested under axisymmetrical conditions.

No ruptured fibers were found in the specimens on inspection after the tests. However, for polyamide fibers, some permanent kinking and local damage was noticed. The prediction of the composite failure stress for both steel and polyamide fibers is made in Fig. 8 using (22). The major principal stress at failure, $\bar{\sigma}_1$, is shown as a function of the confining stress, $\bar{\sigma}_3$ ($\bar{\sigma}_1 = p + R$, $\bar{\sigma}_3 = p - R$). The experimental results came from tests on composite specimens with $\rho = 0.0125$ (1.25%) and $\eta = 40$ (steel fibers), and $\rho = 0.005$ (0.5%) and $\eta = 85$ (polyamide fibers). The internal friction angle for the granular matrix (determined from drained triaxial compression tests) was in the range of 42°–35.9° for specimens tested under confining pressures from 100 to 600 kN/m^2. This is why the predicted failure criteria in Fig. 8 are not straight lines.

The angle of fiber/soil interface friction was determined from pullout experiments in a modified direct shear apparatus (for steel fibers), and from a direct shear of soil over a polyamide sheet, also in a direct shear device. The friction angle is dependent on the normal pressure at the fiber interface and, for steel, was found to be in the range of 24.6°–19.5°, and, for polyamide, in the range of 17.9°–14.7° (normal interface stress changing from approximately 160 to 1,600 kN/m^2). In the interpretation of steel fiber pullout tests, the active stress state in the soil was assumed, inhomogeneities in the mobilization of friction along the fiber were ignored, and the peak value of the pullout force was taken to calculate the interface friction angle (reasonable for short inclusions such as fibers).

The increase in the deviatoric failure stress for fiber-reinforced specimens with respect to the sand tested under identical confining pressure was roughly 20%. This relative increase is smaller when presented in terms of the in-plane invariants R and p since an increase in the deviatoric stress (while confining pressure is constant) also causes an increase in the mean maximum-minimum stress p. While steel fibers with aspect ratio $\eta = 40$ may not seem to be a very effective reinforcement, the theoretical prediction follows the experimental results very closely [Fig. 8(a)]. Table 2 presents the data including the internal friction angle for the granular matrix, φ, and the interface friction angle, φ_w. The friction angle (secant) was calculated from sand samples tested under a given (constant) confining pressure (σ_3), and it is related (in Table 2) to composite mean stress p for which the confining pressure was the same (i.e., φ in column 2 was not calculated from data in columns 1 and 6). The internal friction angle for $p = 203.6$ kN/m^2 was extrapolated. Since tests were performed under a constant confining pressure, mean stress p at failure for reinforced and nonreinforced specimens varied. The magnitude of R for the granular matrix alone, column 6 in Table 2, was therefore interpolated to relate to p in column 1.

Fig. 8(b) presents predictions for sand reinforced with polyamide fibers. There is a tendency to underestimate the actual influence of fiber reinforcement for large mean stresses. In the

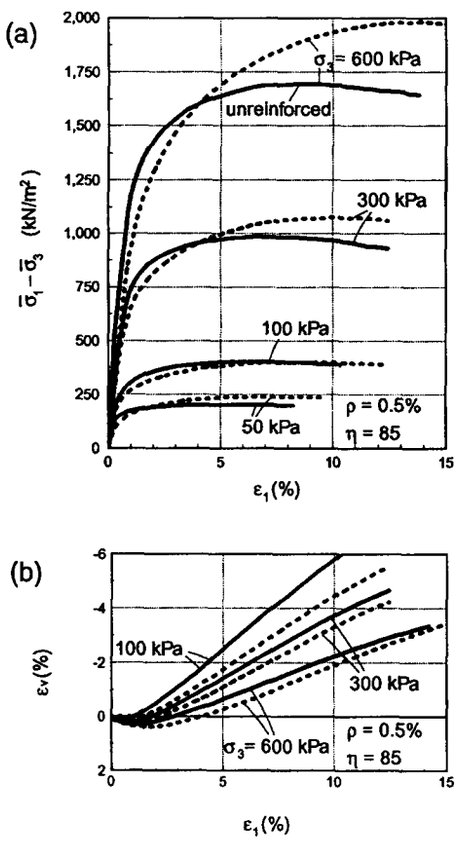

FIG. 6. Triaxial Compression Tests on Sand Reinforced with Polyamide Fibers: (a) Stress-Strain Relation for Different Confining Pressures; (b) Volumetric Strain

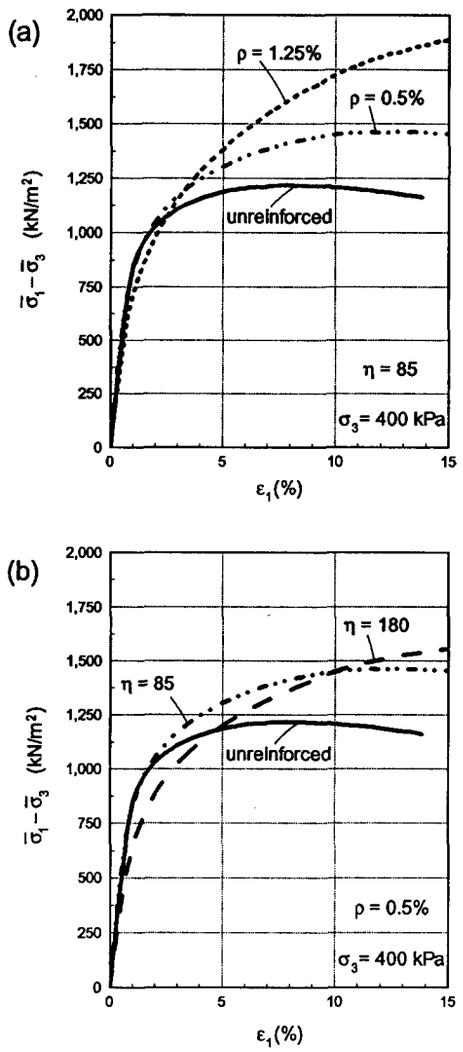

FIG. 7. Stress-Strain Behavior of Polyamide Fiber-Reinforced Sand: (a) Influence of Fiber Content; (b) Effect of Fiber Aspect Ratio

theoretical model the fibers were assumed to be straight inclusions, and a possible source of discrepancies may be in ignoring any effects stemming from local damage (gouging, ploughing) and "serpentine" alignment of fibers (which enhances the soil-fiber interaction). These effects are more pronounced for soft fibers, such as polyamide.

It is fair to conclude that the suggested model is consistent with experimental evidence, but an amount of monofilament fibers up to 1.25% (by volume) is not significant enough to make a meaningful practical improvement. However, a more substantial improvement can probably be expected for fibrillated inclusions with a larger aspect ratio.

FINAL REMARKS

Energy-based homogenization is a viable technique for describing the macroscopic (average) stress at failure for fiber-reinforced granular composites. The particular mixture considered was uniform with respect to both the spatial distribution of fibers and the distribution of fiber orientation. Consequently, the limit condition obtained is isotropic. A piecewise closed-form failure criterion was obtained in terms of the macroscopic (average) stress state. Since the granular matrix was described by the Mohr-Coulomb failure function, the limit condition for the composite is independent of the mean principal stress and can be represented conveniently in terms of the in-plane invariants R (maximum shear stress) and p (mean maximum-minimum principal stress).

The failure criterion consists of two segments: the first one describes failure of the composite due to fiber slip, and the second one is associated with the tensile rupture (or plastic

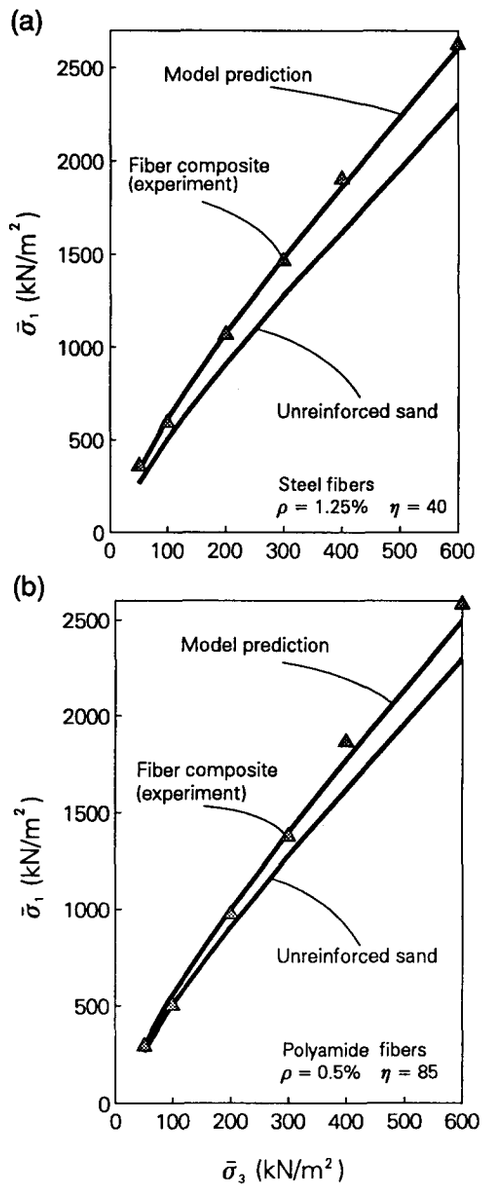

FIG. 8. Comparison of Theoretical and Experimental Failure Criteria: (a) Steel Fiber-Reinforced Sand; (b) Polyamide Fibers

TABLE 2. Failure Stress, Experimental Data, and predictions; ρ = 1.25%, η = 40

Composite stress $(\bar{\sigma}_x + \bar{\sigma}_y)/2$ p (kN/m²) (1)	Sand φ (deg.) (2)	Interface φ_w (deg.) (3)	R (kN/m²) Composite (experiment) (4)	Composite (prediction) (5)	Sand (experiment) (6)
203.6	43	24.6	153.6	150.3	136.3
345.9	42	23	245.9	249.3	228.2
633.1	39.7	22	433.1	434.5	399.7
881.8	38.3	21	581.8	585.5	540.7
1,150.8	37.1	20	750.8	741.6	686.4
1,611.9	35.9	19.5	1,011.9	1,008.4	936.8

flow) of fibers. However, the transition from one mode to another is continuous and smooth (continuous derivative).

Five parameters are needed to theoretically predict the failure stress using the proposed criterion: fiber concentration ρ, fiber aspect ratio η, yield point σ_0, soil/fiber interface friction angle φ_w, and the internal friction angle of the granular matrix φ. For a pure fiber slip failure mode, the failure criterion is independent of the fiber yield stress (although σ_0 was used to present the result in a dimensionless fashion).

For the derived failure criterion to be applicable, the fiber concentration needs to be low enough (say less than 10%) so that the interaction between fibers can be neglected. This is a common limitation of self-consistent schemes of homogenization. The length of fibers needs to be at least one order of magnitude larger than the grain diameter, and the fiber diameter needs to be at least of the same order as the size of sand grains.

The derived failure criterion best predicts the strength of soil reinforced with fibers, which retain their straight shape when placed in soil and loaded (such as steel fibers in a coarse matrix tested here; a coarse matrix is one with a grain size comparable or larger than the fiber diameter). This criterion yields reasonable results for flexible fibers in a coarse matrix, although the prediction could possibly be improved by including the effect of a serpentine alignment of fibers when mixed with a coarse granular soil.

Although the derived failure criterion is consistent with experimental evidence, the amount of monofilament fibers used in tests (up to 1.25% by volume) is not significant enough to make a meaningful practical improvement. The failure criterion derived indicates that fibers may be an effective way for soil reinforcement when mixtures with a larger fiber content or larger aspect ratios are used. Experiments also indicate that the stiffness of the soil prior to failure is affected by the addition of fibers, and, for flexible fibers, it drops down with respect to the stiffness of the granular matrix.

The failure criterion derived is directly applicable in numerical methods for solving boundary-value problems, but it is limited to isotropic mixtures. Future research needs to address the possible anisotropy of the composite (as it is expected to be a practical case when the mixture is compacted with rollers), and the refinement of the criterion for flexible (polymeric) fibers in a coarse base material.

ACKNOWLEDGMENTS

The research presented in this paper was supported by the Air Force Office of Scientific Research, Grant No. F49620-93-1-0192, and by the National Science Foundation, Grant No. CMS9301494. This support is greatly appreciated. The writers would also like to thank P. Lade and J. Yamamuro of The Johns Hopkins University for their help in carrying out the experimental program.

APPENDIX I. DERIVATION OF ENERGY DISSIPATION RATE EXPRESSION

Having assumed that $\bar{\sigma}_n$ can be approximated by p, and noting that $dV = 1/3R_0\, dS$ (Fig. 2), (13) can be written as

$$D_r = 2\frac{\rho\sigma_0}{\pi R_0^2}\left(1 - \frac{1}{4\eta}\frac{\sigma_0}{p\tan\varphi_w}\right)\int_S \langle\dot{\varepsilon}_\theta\rangle\, dS \tag{27}$$

The unit vector normal to the spherical surface in Fig. 2 is

$$\mathbf{n} = \frac{x}{R_0}\mathbf{i} + \frac{y}{R_0}\mathbf{j} + \frac{z}{R_0}\mathbf{k} \tag{28}$$

and the velocity vector is

$$\mathbf{v} = -\dot{\varepsilon}_1 x\mathbf{i} - \dot{\varepsilon}_3 y\mathbf{j} \tag{29}$$

thus the magnitude of the velocity component along $\mathbf{n}$ becomes

$$v_\theta = \mathbf{v}\cdot\mathbf{n} = -\frac{x^2}{R_0}\dot{\varepsilon}_1 - \frac{y^2}{R_0}\dot{\varepsilon}_3 \tag{30}$$

and the strain rate along a fiber identified by coordinates x and y on the sphere's surface in the ordered space is

$$\dot{\varepsilon}_\theta = -\frac{v_\theta}{R_0} = \frac{\dot{\varepsilon}_1 x^2 + \dot{\varepsilon}_3 y^2}{R_0^2} \tag{31}$$

Substituting (31) into (27) one obtains

$$D_r = 2\frac{\rho\sigma_0}{\pi R_0^4}\left(1 - \frac{1}{4\eta}\frac{\sigma_0}{p\tan\varphi_w}\right)\int_S (-\dot{\varepsilon}_1 x^2 - \dot{\varepsilon}_3 y^2)\, dS \tag{32}$$

Because of the definition of $\langle\dot{\varepsilon}_\theta\rangle$ [(12)] a minus sign appears in the integral expression, and S is part of the surface associated with fibers under tension only (ABC, in Fig. 2). The following transformation is used to analytically solve the integral in (32):

$$\int\int_S f(x, y, z)\, dS = \int\int_\Omega f[x, y, z(x, y)]\sqrt{1 + \left(\frac{\partial z}{\partial x}\right)^2 + \left(\frac{\partial z}{\partial y}\right)^2}\, dx\, dy \tag{33}$$

where Ω = projection of area S on the x-y plane (projection of surface ABCA in Fig. 2 on x-y plane). Note that $z = (R_0^2 - x^2 - y^2)^{1/2}$, thus

$$\frac{\partial z}{\partial x} = \frac{-x}{\sqrt{R_0^2 - x^2 - y^2}};\quad \frac{\partial z}{\partial y} = \frac{-y}{\sqrt{R_0^2 - x^2 - y^2}} \tag{34a,b}$$

Eq. (32) now becomes

$$D_r = 2\frac{\rho\sigma_0}{\pi R_0^3}\left(1 - \frac{1}{4\eta}\frac{\sigma_0}{p\tan\varphi_w}\right)\int\int_\Omega (-\dot{\varepsilon}_1 x^2 - \dot{\varepsilon}_3 y^2)\cdot\frac{1}{\sqrt{R_0^2 - x^2 - y^2}}\, dx\, dy \tag{35}$$

Introducing new variables ζ and θ [$\zeta = (x^2 + y^2)^{1/2}$, $\theta = \tan^{-1}(y/x)$], and using (8), the expression in (35) becomes

$$D_r = 2\frac{\rho\sigma_0}{\pi R_0^3}\left(1 - \frac{1}{4\eta}\frac{\sigma_0}{p\tan\varphi_w}\right)\int_0^{R_0}\int_{\theta_0}^{\pi/2}(-\dot{\varepsilon}_1)\frac{\zeta^3}{\sqrt{R_0^2 - \zeta^2}}\cdot\left[\cos^2\theta - \sin^2\theta\tan^2\left(\frac{\pi}{4} + \frac{\varphi}{2}\right)\right]d\zeta\, d\theta \tag{36}$$

where θ_0 is given in (9). The expression in (36) can be analytically integrated to yield

$$D_r = \frac{\rho\sigma_0}{3}M\left(1 - \frac{1}{4\eta}\frac{\sigma_0}{p\tan\varphi_w}\right)\dot{\varepsilon}_1 \tag{37}$$

where M is

$$M = \left(\frac{1}{2} + \frac{\varphi}{\pi} + \frac{1}{\pi}\cos\varphi\right)\tan^2\left(\frac{\pi}{4} + \frac{\varphi}{2}\right) - \frac{1}{2} - \frac{\varphi}{\pi} + \frac{1}{\pi}\cos\varphi \tag{38}$$

APPENDIX II. REFERENCES

Andersland, O. B., and Khattak, A. S. (1979). "Shear strength of kaolinite/fiber soil mixtures." *Proc., Int. Conf. on Soil Reinforcement: Reinforced Soil and Other Techniques; Vol. 1*, 11–16.

Arenicz, R. M., and Chowdhury, R. N. (1988). "Laboratory investigation of earth walls simultaneously reinforced by strips and random reinforcement." *Geot. Testing J.*, 11(4), 241–247.

Budiansky, B. (1965). "On the elastic moduli of some heterogeneous materials." *J. Mech. Phys. Solids*, Vol. 13, 223–227.
de Buhan, P., Mangiavacchi, R., Nova, R., Pellegrini, G., and Salençon, J. (1989). "Yield design of reinforced earth walls by homogenization method." *Géotechnique*, London, England, 39(2), 189–201.
di Prisco, C., and Nova, R. (1993). "A constitutive model for soil reinforced by continuous threads." *Geotextiles and Geomembranes*, Vol. 12, 161–178.
Dvorak, G. J., Rao, M. S. M., and Tarn, J. Q. (1974). "Generalized initial yield surfaces for unidirectional composites." *J. Appl. Mech., Trans. ASME*, Vol. 41, 249–253.
Gray, D. H., and Ohashi, H. (1983). "Mechanics of fiber reinforcement in sand." *J. Geotech. Engrg.*, ASCE, Vol. 109, 335–353.
Hashin, Z. (1964). "Transverse strength." *Evaluation of filament reinforced composites for aerospace structural applications*. N. F. Dow and B. W. Rosen, eds., NASA CR-207, Nat. Aeronautics and Space Admin. (NASA), Washington, D.C., 36–43.
Hashin, Z. (1983). "Analysis of composite materials—a survey." *J. Appl. Mech.*, Trans ASME, Vol. 50, 481–505.
Hill, R. (1965). "A self-consistent mechanics of composite materials." *J. Mech. Phys. Solids*, Vol. 13, 213–222.
Hoare, D. J. (1979). "Laboratory study of granular soils reinforced with randomly oriented discrete fibers." *Proc., Int. Conf. on Soil Reinforcement: reinforced soil and other techniques; Vol. 1*, 47–52.
Lade, P. V. (1977). "Elasto-plastic stress-strain theory for cohesionless soil with curved yield surfaces." *Int. J. Solids Structures*, Vol. 13, 1019–1035.
Leflaive, E., and Liausu, P. (1986). "The reinforcement of soils by continuous threads." *Proc., 3rd Int. Conf. on Geotextiles; Vol. 4*, Gisteldruck, Vienna, Austria, 1159–1162.
Maher, M. H., and Gray, D. H. (1990). "Static response of sands reinforced with randomly distributed fibers." *J. Geotech. Engrg.*, ASCE, 116(11), 1661–1677.
McLaughlin, P. V., and Batterman, S. C. (1970). "Limit behavior of fibrous materials." *Int. J. Solids Struct.*, Vol. 6, 1357–1376.
Michalowski, R. L., and Zhao, A. (1993). "Failure criteria for homogenized reinforced soils and application in limit analysis of slopes." *Proc., Geosynthetics '93*, Industrial Fabrics Assoc. Int., *Vol. 1*, Minneapolis, Minn., 443–453.
Michalowski, R. L., and Zhao, A. (1994). "Failure criteria for fibrous granular composites." *Computer methods and advances in geomechanics*, H. J. Siriwardane and M. M. Zaman, eds., A. A. Balkema, Rotterdam, The Netherlands, Vol. 2, 1385–1390.
Michalowski, R. L., and Zhao, A. (1995). "Limit condition for unidirectionally reinforced soils." *Proc., Numer. Models in Geomech. V*, G. N. Pande, and S. Pietruszczak, A. A. Balkema, Rotterdam, The Netherlands, 237–242.
Mori, T., and Tanaka, K. (1973). "Average stress in matrix and average elastic energy of materials with misfitting inclusions." *Acta Metallurgica*, Vol. 21, 571–574.
Sawicki, A. (1983). "Plastic limit behavior of reinforced earth." *J. Geotech. Engrg.*, ASCE, 109(7), 1000–1005.
Shu, L. S., and Rosen, B. W. (1967). "Strength of fiber-reinforced composites by limit analysis methods." *J. Composite Mat.*, Vol. 1, 366–381.
Waldron, L. J. (1977). "The shear resistance of root-permeated homogeneous and stratified soil." *Soil Sci. Soc. Am. J.*, Vol. 41, 843–849.
Wu, T. H., McKinnell W. P. III, and Swanston, D. N. (1979). "Strength of tree roots and landslides on Prince of Wales Island, Alaska." *Can. Geotech. J.*, Ottawa, Canada, 16(1), 19–33.

APPENDIX III. NOTATION

The following symbols are used in this paper:

D = energy dissipation rate in composite;
d = energy dissipation rate in a single fiber;
e = void ratio;
G = specific gravity;
l = fiber length;
p = average maximum-minimum stress in composite;
R = radius of Mohr stress circle;
R_0 = radius of the integration sphere;
r = fiber radius;
s = fiber slip length;
V = representative volume;
$\dot{\varepsilon}_{ij}$ = strain rate;
$\dot{\varepsilon}_\theta$ = strain rate in the direction of fiber;
η = fiber aspect ratio;
ρ = volumetric fiber content (fiber concentration);
ρ_w = fiber concentration by weight;
$\bar{\sigma}_{ij}$ = macroscopic stress-state tensor;
σ_n, $\bar{\sigma}_n$ = stress normal to fiber surface, average value;
σ_0 = fiber yield stress;
φ = internal friction angle; and
φ_w = sand/fiber interface friction angle.